

## RESEARCH ARTICLE

# Energy layer optimization via energy matrix regularization for proton spot-scanning arc therapy

Gezhi Zhang<sup>1</sup> | Haozheng Shen<sup>1</sup> | Yuting Lin<sup>2</sup> | Ronald C Chen<sup>2</sup> | Yong Long<sup>1</sup> | Hao Gao<sup>2</sup>

<sup>1</sup>University of Michigan-Shanghai Jiao Tong University Joint Institute, Shanghai Jiao Tong University, Shanghai, China

<sup>2</sup>Department of Radiation Oncology, University of Kansas Medical Center, Kansas City, Missouri, USA

**Correspondence**

Yong Long, University of Michigan-Shanghai Jiao Tong University Joint Institute, Shanghai Jiao Tong University, Shanghai, China  
Email: [yong.long@sjtu.edu.cn](mailto:yong.long@sjtu.edu.cn)

**Funding information**

NIH, Grant/Award Numbers: R37CA250921, R01CA261964

**Abstract**

**Purpose:** Spot-scanning arc therapy (SPArc) is an emerging proton modality that can potentially offer a combination of advantages in plan quality and delivery efficiency, compared with traditional IMPT of a few beam angles. Unlike IMPT, frequent low-to-high energy layer switching (so called switch-up (SU)) can degrade delivery efficiency for SPArc. However, it is a tradeoff between the minimization of SU times and the optimization of plan quality. This work will consider the energy layer optimization (ELO) problem for SPArc and develop a new ELO method via energy matrix (EM) regularization to improve plan quality and delivery efficiency.

**Methods:** The major innovation of EM method for ELO is to design an EM that encourages desirable energy-layer map with minimal SU during SPArc, and then incorporate this EM into the SPArc treatment planning to simultaneously minimize the number of SU and optimize plan quality. The EM method is solved by the fast iterative shrinkage-thresholding algorithm and validated in comparison with a state-of-the-art method, so-called energy sequencing (ES).

**Results:** EM is validated and compared with ES using representative clinical cases. In terms of delivery efficiency, EM had fewer SU than ES with an average of 35% reduction of SU. In terms of plan quality, compared with ES, EM had smaller optimization objective values and better target dose conformality, and generally lower dose to organs-at-risk and lower integral dose to body. In terms of computational efficiency, EM was substantially more efficient than ES by at least 10-fold.

**Conclusion:** We have developed a new ELO method for SPArc using EM regularization and shown that this new method EM can improve both delivery efficiency and plan quality, with substantially reduced computational time, compared with ES.

**KEYWORDS**

energy layer optimization, IMPT, SPArc

## 1 | INTRODUCTION

Proton arc therapy was developed in late 90s with passive scattering,<sup>1,2</sup> which has recently revived into spot-scanning arc therapy (SPArc) by Ding et al.<sup>3</sup> as an emerging proton modality that can potentially offer a combination of advantages in plan quality and delivery efficiency,<sup>4–7</sup> compared with traditional IMPT of a few

beam angles. This work concerns about the energy layer optimization (ELO) problem for SPArc.

The need of ELO for SPArc is motivated by the fact that the low-to-high energy layer switching (i.e., switch-up (SU)) time is much longer than the high-to-low energy layer switching (i.e., switch-down (SD)) time, for example, 5 s versus 0.5 s. The SU is usually not an issue for IMPT of fixed beam angles because <sup>1</sup> energy

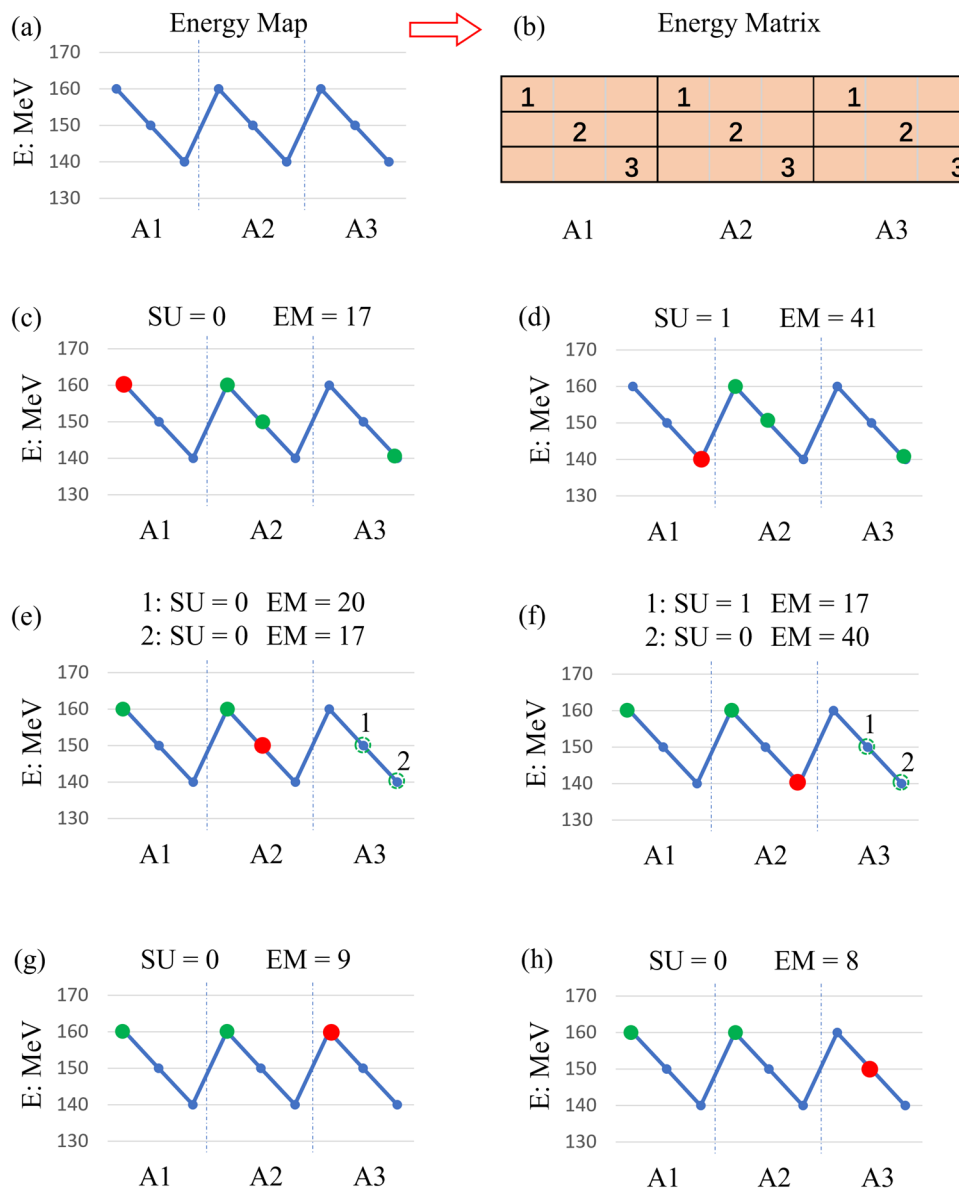


**FIGURE 1** P1–P3 principles behind energy matrix regularization. (a) Energy map of 3 beam angles A1–A3; (b) energy matrix  $M$  corresponding to this energy map. P1 is demonstrated by comparing (c) and (d): the energy matrix encourages the selection of high-energy layers (i.e., 160 instead of 140 MeV for A1 with smaller EM in (c)) for minimizing SU (i.e., smaller SU in (c)). P2 is illustrated by comparing (e) and (f):  $M$  encourages the selection of high-energy layers (i.e., 150 instead of 140 MeV for A2 in (e)) to have more degrees of freedom for optimizing plan quality without increasing SU (i.e., A3 can be filled with either 150 or 140 MeV without increasing SU in (e), while only 140 MeV for A3 does not increase SU for in (f)). P3 is explained by comparing (g) and (h):  $M$  penalizes the selection of only high-energy layers (i.e., 160 MeV for all angles A1–A3 with larger EM in (g)) to have diversified energy layers for the purpose of optimizing plan quality

layers are delivered from high to low within each beam angle so that SU does not occur within an angle, and (2) the angle switching takes time anyway so that SU may not require additional time even it occurs between angles. However, the SU can be a limiting factor for delivery efficiency of SPARC because ideally the beam can be constantly delivering while the gantry angle is continuously changing during SPARC. Without proper reduction of SU, the gantry may need to stop frequently to wait for beam delivery, or beam delivery may need

to be skipped for many arcs in order to wait for SU to complete before resuming beam delivery. Therefore, the minimization of SU is important for SPARC, in terms of both delivery efficiency and plan quality.

While Ding's method<sup>3</sup> was heuristic, Gu et al.<sup>8</sup> proposed an ELO method with a rigorous problem formulation and method derivation, using so-called energy sequencing (ES) regularization (ESR) to minimize SU while optimizing plan quality. However, in order for ES to function, ES imposes the optimization constraint "one

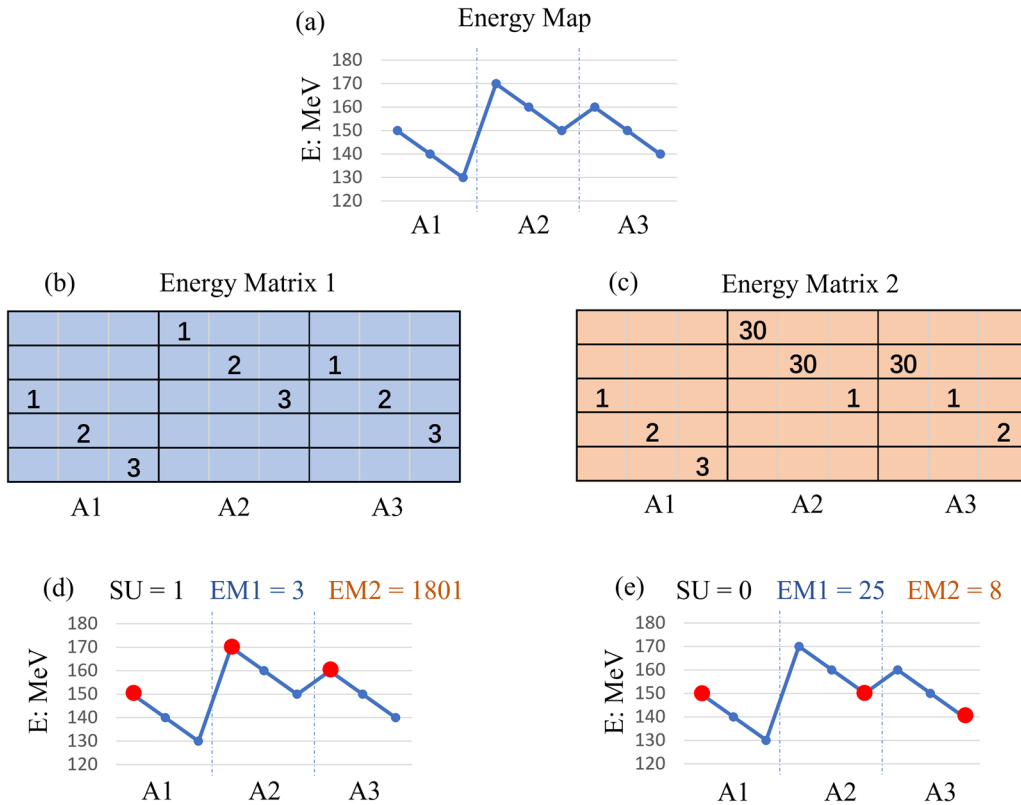


**FIGURE 2** P4 principle behind energy matrix regularization. (a) Energy map. (b) Energy matrix M1 (without barrier constraint); M1 is local to each beam angle in the sense that the M1 matrix value (i.e., 1, 2, 3) corresponds to the descending order of energies per angle. (c) Energy matrix M2 (with barrier constraints); owing to the barrier constraints (i.e., the matrix values of M2 equal to a much larger number 30 at 170 and 160 MeV for A2 and 160 MeV for A3), M2 is nonlocal in the sense that the M2 matrix value is also determined by the descending order of energies for all angles. P4 is demonstrated by comparing (d) and (e): P4 introduces barrier constraints to minimize SU; without barrier constraint, M1 falsely chooses SU = 1 (d) over SU = 0 (e), because SU = 1 has smaller EM1; with barrier constraints, M2 correctly chooses SU = 0 (e) over SU = 1 (d), because SU = 0 has smaller EM2. Note that the barrier constraint value 30 could have been set to a different value rather than 30, as long as it is sufficiently larger than the rest of matrix values

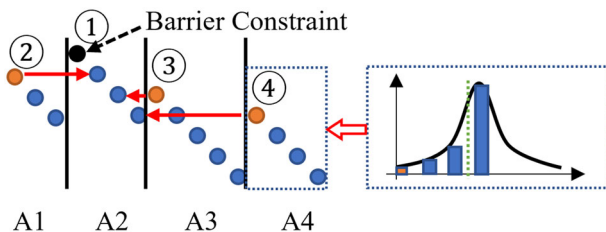


**FIGURE 3** Generation of energy matrix. First, the leading energy layer (with the largest energy) per beam angle is located (orange and black circles in the figure). Second, the largest leading energy layer is identified (the black circle) and the submatrix (i.e., A2 that starts from the first row of  $M$ ) for this angle (the so-called benchmark angle) is determined. Third, for each of the rest of beam angles (A1, A3, A4), the leading energy layer is aligned to A2 (e.g., the submatrix for A1 starting from the row in A2 of the same energy). Fourth, the barrier constraints (with substantially larger values for the penalization purpose) are assigned for the layers with larger energy (the black circle) than the leading energy layer of A1. Last, diagonal matrix values for each submatrix (without barrier constraint) are calculated in the descending energy order (larger matrix value for smaller energy) via the Gaussian distribution

energy layer per beam angle” (here each beam angle during SPARC optimization is after discretization and represents an angular segment or control point during SPARC delivery), which seems practically unnecessary and limits optimization degrees of freedom for plan quality. Because the optimization solution space with the constraint “one energy layer per beam angle” is a subset of the solution space without this constraint, the optimal plan quality under this constraint is usually worse than the plan quality that can be achieved with “multiple energy layers per beam angle.”<sup>6</sup> On the other hand, the ESR involves the updates of several ES matrices each iteration, which is computationally expensive. Inspired by SPARC<sup>3</sup> and ES,<sup>8</sup> this work will develop a new ELO method for SPARC using energy matrix (EM) regularization (EMR). Relative to ES, EM does not need to be restricted by the aforementioned optimization constraint so that more than one energy layer per beam angle is allowed in order to improve plan quality. It will be shown that EM can further reduce number of SU, improve plan quality, and enhance computational efficiency from ES.

**TABLE 1** Comparison of dosimetric parameters between ES and EM

	Quantity (Unit)	ES	EM
Abdomen	CI	0.83	0.86
	HI	9.38	7.30
	$D_{\text{mean,bowel}}$ (Gy)	2.14	1.69
	$D_{\text{mean,body}}$ (Gy)	0.47	0.42
	$f$	0.04	0.01
Brain	CI	0.53	0.84
	HI	9.27	8.59
	$D_{\text{mean,brainstem}}$ (Gy)	3.32	2.77
	$D_{\text{mean,body}}$ (Gy)	0.93	0.95
	$f$	1.41	1.29
HN	CI	0.59	0.79
	HI	13.65	9.94
	$D_{\text{mean,larynx}}$ (Gy)	4.89	4.62
	$D_{\text{mean,body}}$ (Gy)	2.00	1.86
	$f$	0.04	0.04
Lung	CI	0.63	0.83
	HI	15.14	9.34
	$D_{\text{mean,heart}}$ (Gy)	1.02	0.89
	$D_{\text{mean,body}}$ (Gy)	2.39	2.24
	$f$	0.03	0.02

Optimized planning objective value  $f$ , CI, and HI are unitless

**TABLE 2** Comparison of plan delivery time between ES and EM

	Quantity	ES	EM
Abdomen	SU	36	13
	SD	28	48
	$T_E$	215	100
	$T_B$	92	40
	$T$	307	140
Brain	SU	31	26
	SD	31	43
	$T_E$	189	169
	$T_B$	63	48
	$T$	252	217
HN	SU	35	24
	SD	26	58
	$T_E$	208	167
	$T_B$	252	192
	$T$	460	359
Lung	SU	32	24
	SD	32	47
	$T_E$	195	160
	$T_B$	220	179
	$T$	415	339

The values of energy switching time  $T_E$ , spot delivery time  $T_B$ , and total plan delivery time  $T = T_E + T_B$  have the unit of second.

## 2 | METHODS AND MATERIALS

### 2.1 | Notations

Let  $B$  be the number of beam angles during SPArc plan optimization, and  $E_b$  the number of energy layers in the  $b$ th angle. For the convenience of presentation, energy layer distribution for all beam angles (e.g., Figure 1(a)) is called the energy map.

Note that the modeling of SPArc in many fixed beam angles here is a mathematical approximation or discretization of arc delivery, which does not mean that SPArc is delivered only at those fixed beam angles. In the actual delivery, the gantry angle varies continuously, for which each beam angle in the presented model corresponds to an angular segment  $2\pi/B$  or control point.

The vector  $x$  denotes intensities or the number of particles per spot for all spots from all angles,  $x_b$  all spots for the  $b$ th angle, and  $x_{be}$  all spots with the  $e$ th energy layer in the  $b$ th angle. That is

$$x = \begin{bmatrix} x_1 \\ x_2 \\ \vdots \\ x_b \\ \vdots \\ x_B \end{bmatrix}, x_b = \begin{bmatrix} x_{b1} \\ x_{b2} \\ \vdots \\ x_{be} \\ \vdots \\ x_{bE_b} \end{bmatrix}, x_{be} = \begin{bmatrix} x_{be1} \\ x_{be2} \\ \vdots \\ x_{ben} \\ \vdots \\ x_{beN_{be}} \end{bmatrix} \quad (1)$$

where  $N_{be}$  is the length of  $x_{be}$ , that is, the number of spots in the  $e$ th energy layer of the  $b$ th angle.

To group the spots per energy layer, we introduce the scalar  $y_{be}$  as the sum of all elements in  $x_{be}$ , the vector  $y_b$  as the concatenation of  $y_{be}$  corresponding to the  $b$ th angle, and  $y$  that consists of all  $y_b$ 's from all angles. That is

$$y = \begin{bmatrix} y_1 \\ y_2 \\ \vdots \\ y_b \\ \vdots \\ y_B \end{bmatrix}, y_b = \begin{bmatrix} y_{b1} \\ y_{b2} \\ \vdots \\ y_{be} \\ \vdots \\ y_{bE_b} \end{bmatrix}, y_{be} = \sum_{i=1}^{N_{be}} x_{bei} \quad (2)$$

In matrix representation,  $y = Wx$ , where  $W$  is a summation matrix that sums up  $x$  per energy layer.

### 2.2 | Energy layer optimization

We start the formulation of ELO by giving the dose fidelity term

$$f(x) = \sum_{S \in \Omega} w_s \|A_s x - d_s\|_2^2, \quad (3)$$

where  $\Omega$  is a set of different structures including the treatment planning target PTV and organs-at-risk (OAR),  $d_s$  is the constraint dose,  $A_s$  is the dose influence matrix, and  $w_s$  is the objective weight, corresponding to the  $s$ th structure. Note that  $\Omega$  depends on  $x$  and needs to be updated during plan optimization iterations, for dose-volume constraints<sup>9–11</sup>: for example, for dose-volume constraint  $D_{50\%} < 30$  Gy, if the volume of  $\geq 30$  Gy is 60% (which is more than 50%),  $\Omega$  for this constraint will include the 10% dose-violating voxels of the smallest dose for dose minimization.

To benchmark and compare with the ES method, the EM method adopts the similar ELO formulation to ES<sup>8</sup>

$$\min_x F(x) = f(x) + GS(x) + \text{LOG}(y) + \text{EMR}(y) \quad (4)$$

subject to  $x \geq 0, y = Wx$

where

$$\begin{aligned} f(x) &= \|Ax - d\|_2^2, \\ GS(x) &= \alpha \sum_{b=1}^B \sum_{e=1}^{E_b} w_{be} \|x_{be}\|_2, \\ \text{LOG}(y) &= -\beta \sum_{b=1}^B \log \left( \sum_{e=1}^{E_b} y_{be} \right), \\ \text{EMR}(y) &= \gamma \|MS \end{aligned} \quad (5)$$

The first term  $f$  is dose fidelity term Equation (3), where, without loss of generality, Equation (3) is denoted by a simplified version in Equation (5). The second term GS is group-sparsity regularization to minimize the number of energy layers with energy-layer-dependent weighting  $w_{be}$ .<sup>12</sup> The third term LOG uses a log barrier function to promote that each angle has at least one energy layer, since the GS alone may generate the energy map with angles of empty energy layers.<sup>8</sup> The fourth term is the EMR with the EM  $M$ .

The difference between ES and EM methods is that the ESR is replaced by the EMR in Equation (4). In the EMR term Equation (5),  $S$  is a sigmoid function that binarizes  $y$  to capture energy SU for the purpose of EMR, that is,  $S(y) = 2/(1 + e^{-y}) - 1$ .

Note that the necessity of L2 norm (i.e., sum of least squares) in EMR can be explained by comparing Figures 1(g) and 1(h). The EM method can minimize the number of SU to improve the delivery efficiency of SPARC, using the properly designed EM, that is,  $M$  in Equation (5), that will be explained next.

## 2.3 | EMR: principle

This section discusses the principles for designing the EM (P1–P4), and the next section will provide the algorithm for generating the EM.

To mimic the delivery of SPARC, energy layers per beam angle in the energy map (e.g., Figure 1(a)) are sorted in the descending order of proton energies, that is, the energy layers are delivered always from high to low energies (e.g., for the 2nd angle A2 in Figure 1(c)), while the energy SU can occur at the transition of beam angles (e.g., from the 1st angle A1 to the 2nd angle A2 in Figure 1(d)). Since the energy SU (from low to high) takes much longer than the SD (from high to low), smaller number of SU often implies faster delivery of SPARC.

For minimizing the number of SU and at the same time optimizing the plan quality, the EM  $M$  is designed in such a way with

- (P1) the selection of high-energy layers to minimize SU for the purpose of efficient plan delivery (e.g., by comparing Figures 1(c) and 1(d));
- (P2) the selection of high-energy layers to have more degrees of freedom for optimizing plan quality without increasing SU (e.g., by comparing Figures 1(e) and (f));
- (P3) the penalization of the selection of only high-energy layers to have diversified energy layers for the purpose of optimizing plan quality (e.g., by comparing Figures 1(g) and (h));
- (P4) the introduction of barrier constraints (e.g., Figure 2(c)) to minimize SU (e.g., by comparing Figures 2(d) and (e)).

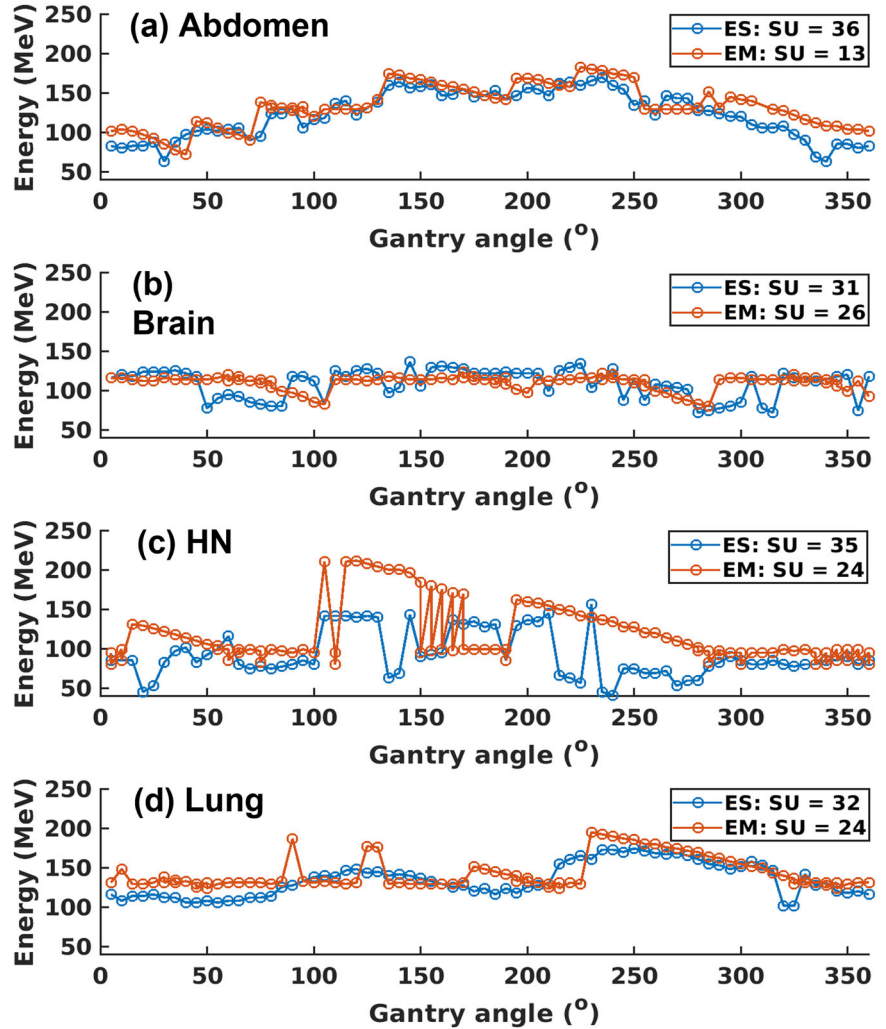
First, we will illustrate the use of  $M$  matrix via two examples (Figures 1 and 2): P1–P3 will be explained via Figure 1, and P4 will be explained via Figure 2. Then, we will provide the algorithm (Figure 3) to determine  $M$ .

Because the number of SU is determined by “*which energy layers to use*” rather than specific spot values per energy layer, the  $M$  matrix concerns about the binarized  $y$ :  $y_{be} = 1$  when the  $e$ th energy layer of the  $b$ th beam angle is used (i.e., with at least one nonzero spot to be delivered);  $y_{be} = 0$  otherwise. Throughout this section (including Figures 1 and 2), EM refers to the value of EMR term in Equation (5) acting on the binarized  $y$  without  $\gamma$ , that is,  $\text{EM} = \|My\|^2$  and strictly speaking  $y$  corresponds to  $S(y)$  after the sigmoid transform.

An example of EM  $M$  is provided in Figure 1(b), which corresponds to the energy map in Figure 1(a). The optimization degrees of freedom in this example consist of three beam angles (A1–A3), each of which has three energy layers (140, 150, 160 MeV). The beam angles are sorted in the order of actual delivery, and the energy layers are arranged in the order of descending energy values.

To illustrate P1, let us consider Figures 1(c) and 1(d), where active energy layers (i.e.,  $y_{be} = 1$ ) are denoted by red and green dots. In terms of SU, since there is no SU in Figure 1(c),  $\text{SU} = 0$ ; since there is a SU from A1 to A2 in Figure 1(d),  $\text{SU} = 1$ . In terms of EMR, in Figure 1(c),

**FIGURE 4** Comparison of energy-layer delivery trajectories between ES (blue) and EM (red)



$y = [1\ 0\ 0\ 1\ 1\ 0\ 0\ 0\ 1]^T$  and thus  $EM = 17$ ; in Figure 1(d),  $y = [0\ 0\ 1\ 1\ 1\ 0\ 0\ 0\ 1]^T$  and thus  $EM = 41$ . Therefore, the EM  $M$  encourages the selection of high-energy layers (i.e., 160 instead of 140 MeV for A1 with smaller  $EM = 17$  than  $EM = 41$ ) for minimizing SU (i.e.,  $SU = 0$  instead of  $SU = 1$ ).

To illustrate P2, let us consider Figures 1(e) and 1(f). In terms of SU, when 150 MeV is active in A2 (Figure 1(e)), either 150 or 140 MeV can be active in A3 without increasing SU; when 140 MeV is active in A2 (Figure 1(f)), only 140 MeV can be active in A3 without increasing SU. In terms of EMR, in Figure 1(e),  $y = [1\ 0\ 0\ 1\ 1\ 0\ 0\ 1\ 0]^T$  and  $EM = 20$  if 150 MeV is active in A3, while  $y = [1\ 0\ 0\ 1\ 1\ 0\ 0\ 0\ 1]^T$  and  $EM = 17$  if 140 MeV is active in A3; in Figure 1(f),  $y = [1\ 0\ 0\ 1\ 0\ 1\ 0\ 1\ 0]^T$  and  $EM = 17$  if 150 MeV is active in A3, while  $y = [1\ 0\ 0\ 1\ 0\ 1\ 0\ 1\ 0]^T$  and  $EM = 40$  if 140 MeV is active in A3. Therefore,  $M$  encourages the selection of high-energy layers (i.e., 150 instead of 140 MeV for A2 in Figure 1(e)) to have more rooms for optimizing plan quality without increasing SU (i.e., A3 can be filled with either 150 or 140 MeV without increasing SU in Figure 1(e), while only 140 MeV for A3 does not increase SU for in Figure 1(f)).

To illustrate P3, let us consider Figures 1(g) and 1(h). In terms of EMR, in Figure 1(g),  $y = [1\ 0\ 0\ 1\ 0\ 0\ 1\ 0\ 0]^T$  and thus  $EM = 9$ ; in Figure 1(h),  $y = [1\ 0\ 0\ 1\ 0\ 0\ 0\ 1\ 0]^T$  and thus  $EM = 8$ . Therefore,  $M$  penalizes the selection of only high-energy layers (i.e., 160 MeV for all angles A1–A3 with larger EM in Figure 1(g)) to have diversified energy layers for the purpose of optimizing plan quality.

Note that the EM in Figure 1(b) is local in the sense its matrix value only depends on the local ordering of energy layers per beam angle and is independent of the global ordering energy layers from all beam angles. This locality can be problematic, when the energy map has different energy-layer distribution per beam angle (e.g., Figure 2(a)). To incorporate the globality (in the ordering energy layers) into EM, barrier constraints are introduced and explained next.

To illustrate P4 on barrier constraints, let us consider Figure 2. The optimization degrees of freedom (Figure 2(a)) in this example consist of energy layers (150, 140, and 130 MeV) for A1, energy layers (170, 160, and 150 MeV) for A2, and energy layers (160, 150, and 140 MeV) for A3. The EM  $M1$  (Figure 2(b)) is similar to the previous one in Figure 1:  $M1$  is local to each beam

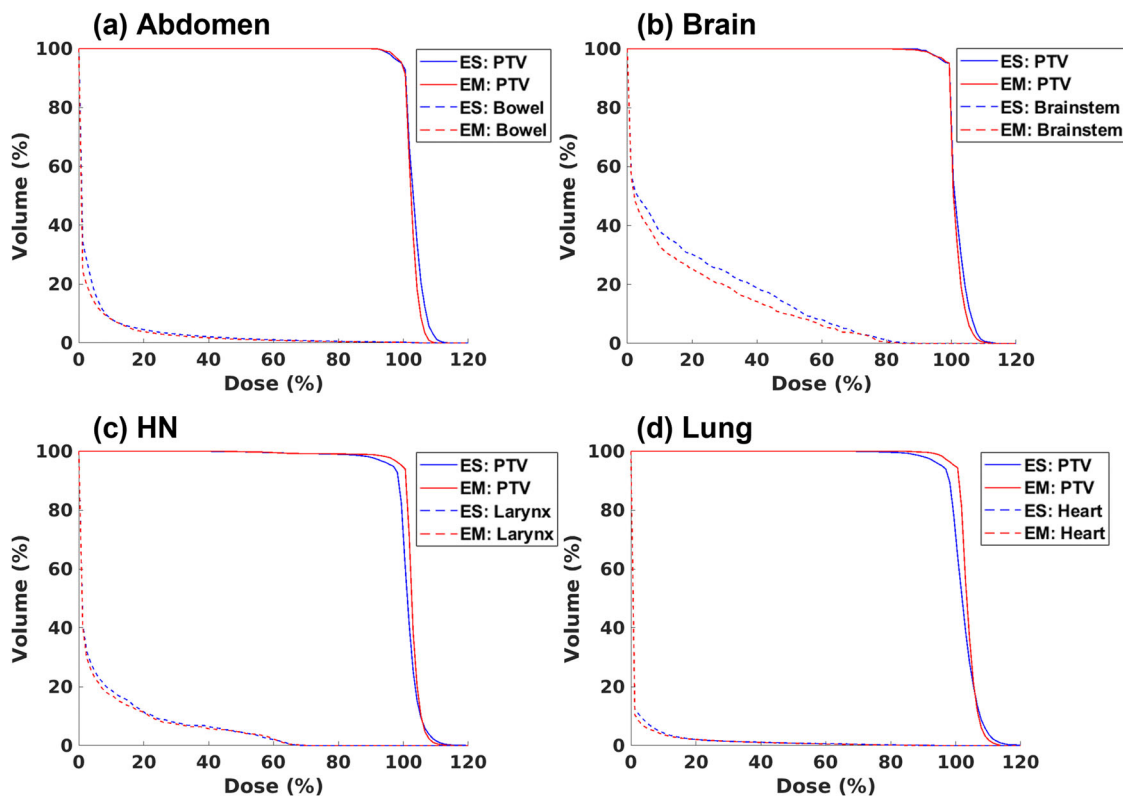


FIGURE 5 DVH plots. Blue solid line: PTV of ES; blue dashed line: OAR of ES; red solid line: PTV of EM; red dashed line: OAR of EM

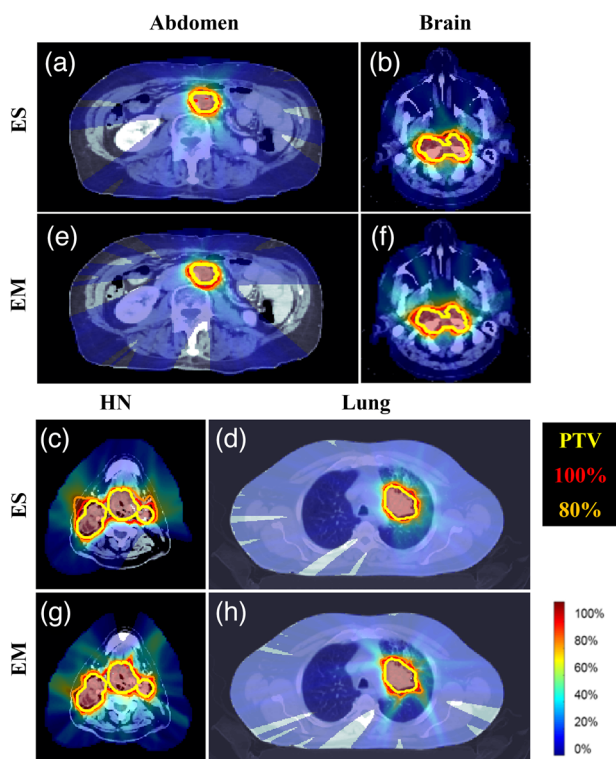


FIGURE 6 Dose plots. (a–d): ES; (e–h): EM. (a and e): abdomen; (b and f) brain; (c and g): HN; (d, h): lung. The dose plot window is [0%, 110%]. PTV, 100% isodose line and 80% isodose line are highlighted

angle in the sense that the M1 matrix value (i.e., 1, 2, 3) corresponds to the descending order of energies per angle. On the other hand, the EM M2 (Figure 2(c)) has the barrier constraints, that is, the matrix values of M2 equal to a much larger number 30 (here 30 is the barrier constraint value, which could have been set to a different value rather than 30, as long as it is sufficiently larger than the rest of values, e.g., by 10-fold) at 170 and 160 MeV for A2 and 160 MeV for A3; as a result, M2 is nonlocal in the sense that the M2 matrix value also accounts for the descending order of energies for all angles. In terms of SU, since there is a SU from A1 to A2 in Figure 2(d),  $SU = 1$ ; since there is no SU in Figure 2(e),  $SU = 0$ . In terms of EMR, in Figure 2(d),  $y = [0 \ 0 \ 1 \ 0 \ 0 \ 1 \ 0 \ 0 \ 0 \ 0 \ 1 \ 0 \ 0 \ 0]^T$  (there are 15 elements because there are five different energy layers 170, 160, 150, 140, and 130 MeV, and three angles; for each angle, 1 implies the energy available for optimization and 0 otherwise) and thus  $EM1 = 3$ ,  $EM2 = 1801$ ; in Figure 2(e),  $y = [0 \ 0 \ 1 \ 0 \ 0 \ 0 \ 0 \ 1 \ 0 \ 0 \ 0 \ 0 \ 0 \ 1 \ 0]^T$  and thus  $EM1 = 25$ ,  $EM2 = 8$ . Therefore, without barrier constraint, M1 falsely chooses  $SU = 1$  over  $SU = 0$ , because  $SU = 1$  has smaller  $EM1$ ; with barrier constraints, M2 correctly chooses  $SU = 0$  over  $SU = 1$ , because  $SU = 0$  has smaller  $EM2$ . The purpose of barrier constraint is to delocalize the ordering per angle by giving a sufficiently large weighting (e.g., 30 in this example), so that the EMR correctly penalizes the SU.

## 2.4 | EMR: algorithm

In this section, we will provide the algorithm to determine  $M$  for general energy map, which is illustrated in Figure 3. The algorithm consists of two major steps: (S1) to determine the location of nonzero matrix elements of  $M$ ; (S2) to calculate the values for these nonzero matrix elements.

Regarding S1, the columns of  $M$  are arranged for angles in the order of beam scanning, for energy layers per angle in the order of descending energy values. To determine the rows of  $M$ , first, the leading energy layer (with the largest energy) per beam angle is located (e.g., orange and black circles in Figure 3). Then, the largest leading energy layer is identified (e.g., the black circle in Figure 3) and the submatrix (e.g.,  $A_2$  that starts from the first row of  $M$  in Figure 3) for this angle (the so-called benchmark angle) is determined. Next, for each of the remaining beam angles (e.g.,  $A_1$ ,  $A_3$ , and  $A_4$  in Figure 3), the leading energy layer is aligned to the benchmark angle (e.g., the submatrix for  $A_1$  starting from the row in  $A_2$  of the same energy in Figure 3); within each submatrix per beam angle, the nonzero elements are consecutively placed on the diagonal, starting from the first nonzero element that is already aligned to the benchmark angle. The process of S1 can also be illustrated using Figure 2: first because  $A_2$  has the largest leading energy layer, which is 170 MeV,  $A_2$  is the benchmark angle; then  $A_1$  and  $A_3$  are aligned to  $A_2$  to form the EM in Figure 2(c), that is, to position the leading energy layer 150 MeV of  $A_1$  in the same row as 150 MeV of  $A_2$ , and that is, to position the leading energy layer 160 MeV of  $A_3$  in the same row as 160 MeV of  $A_2$ . Note that the process of S1 is independent of the delivery order of beam angles. For example, since the benchmark angle is the angle with the largest leading energy layer, the benchmark angle remains the same even though the starting angle during SPARC delivery is changed.

Regarding S2, first, to remove the locality of EM, we identify the elements for barrier constraints (i.e., with substantially larger values for the penalization purpose), which are the energy layers with larger energy (e.g., the black circle in Figure 3) than the leading energy layer of  $A_1$ . Then, we determine the rest of diagonal matrix values for each submatrix (without barrier constraint) based on the descending energy order (larger matrix value for smaller energy) via the following Gaussian distribution

$$f(x) = \frac{1}{\sqrt{2\pi\sigma}} \exp\left(-\frac{(x-\mu)^2}{2\sigma^2}\right), \quad x \leq \mu. \quad (6)$$

Here,  $x$  is the local ordering of energy layers per angle (after Barrier constraints are assigned), for example,  $x = 1$  for the energy layer of the largest energy;  $\mu$  is set to be the number of energy layers (without barrier

constraints) per angle; the barrier constant is set to be 10 times of the largest Gaussian values of all angles;  $\sigma = 5$  in this study.

## 2.5 | Optimization algorithm

Since ES was solved by the Fast Iterative Shrinkage-Thresholding Algorithm (FISTA),<sup>13</sup> the optimization algorithm for solving EM here is also based on FISTA, for the purpose of fair comparison with ES, although EM or ES can also be efficiently solved by other methods such as Alternating Direction Method of Multipliers (ADMM).<sup>14,15</sup>

To solve Equation (4) using FISTA, the optimization problem Equation (4) is reformulated as

$$\min_x f(x) + g(x), \quad (7)$$

where

$$\begin{aligned} f(x) &= \|Ax - d\|_2^2 - \beta W_b^T L(W_e x) + \gamma \|MS(Wx)\|_2^2 \\ g(x) &= \alpha \sum_{b=1}^B \sum_{e=1}^{E_b} w_{be} \|x_{be}\|_2 + I_{\geq 0}(x) \end{aligned} \quad (8)$$

Here,  $W$  is the summation matrix that sums up  $x$  per energy layer, that is,  $Wx = \sum_i x_{bei}$ ;  $W_e$  is the summation matrix that sums up  $x$  from all energy layers per beam angle, that is,  $W_e x = \sum_{ei} x_{bei}$ ;  $W_b$  is the summation vector that sums up  $x$  from all beam angles, that is,  $W_b^T x = \sum_b x_b$ ;  $L$  and  $S$  are element-wise functions,  $L(u) = [l(u_1), \dots, l(u_n), \dots, l(u_B)]^T$  with  $l(x) = -\log(x)$ , and  $S(u) = [s(u_1), \dots, s(u_n), \dots, s(u_{N_{be}})]^T$ , and  $s(x) = \frac{2}{1+e^{-x}} - 1$ .  $I_{\geq 0}$  is an indicator function defined as:

$$I_{\geq 0}(x) = \begin{cases} x & \text{if } x \geq 0 \\ \infty & \text{otherwise} \end{cases} \quad (9)$$

Then the gradient of  $f$  is given by

$$\begin{aligned} \nabla f(x) &= 2A^T(Ax - d) - \beta L'(W_e x) W_e^T \\ &\quad + 2\gamma [MS(Wx)]^T [MS'(Wx)] W^T \end{aligned} \quad (10)$$

Here,  $L'$  and  $S'$  are derivatives for  $L$  and  $S$  respectively, with  $l'(x) = -\frac{1}{x}$ , and  $s'(x) = \frac{2e^{-x}}{(1+e^{-x})^2}$ ;  $W^T$  is the transpose of  $W$ , that is,  $x_{bei} = W^T y_{be}$ , where the value of  $y_{be}$  is projected to all spots on this energy layer;  $W_e^T$  is the transpose of  $W_e$ , that is,  $x_{bei} = W_e^T y_b$ , where the value of  $y_b$  is projected to all spots on this beam angle.

The proximal operator of  $g(x)$  has analytical formula<sup>16</sup>

$$\text{prox}_{t\|\cdot\|_2}(x) = \text{prox}_{t\|\cdot\|_2}(\max(x, 0))$$



$$= x - x \cdot \min \left( \frac{t}{\|\max(x, 0)\|_2}, 1 \right) \quad (11)$$

The FISTA algorithm for solving EM is summarized in the following. The parameters  $\alpha$ ,  $\beta$ , and  $\gamma$  are manually chosen case by case. Their values are determined based on the rule of thumb to minimize the number of SU while the plan quality is still preserved. For fair comparison, the values of  $\alpha$ ,  $\beta$ , and  $s$  are the same between ES and EM.

---

**ALGORITHM:** FISTA for solving EM

---

Initialize:  $M, \alpha, \beta, \gamma, x_0, t_0, s, N$

for  $k = 1, 2, \dots, N$

$$\nabla f(x_{k-1}) = 2A^T(Ax_{k-1} - d) - \beta L'(W_e x_{k-1}) W_e^T + 2\gamma [MS(Wx_{k-1})]^T [MS'(Wx_{k-1})] W^T$$

$$y = \text{prox}_{s\|\cdot\|_2}(x_{k-1} - s\nabla f(x_{k-1}))$$

$$t_k = \frac{1 + \sqrt{1 + 4t_{k-1}^2}}{2}$$

$$x_k = y + \left( \frac{t_{k-1} - 1}{t_k} \right) (y - x_{k-1})$$

end for

---

## 2.6 | Materials

The new method (“EM”) was validated in comparison with a state-of-the-art method (“ES”), using abdomen (2.2 Gy  $\times$  25 fractions), brain (2 Gy  $\times$  10 fractions), head-and-neck (HN) (2.12 Gy  $\times$  33 fractions), and lung (2 Gy  $\times$  30 fractions) cases. For optimizing plan quality, first we solved ES and EM (Equation 4) with all regularization terms for selecting energy layers; then, we solved Equation (4) with the dose-fidelity term only on selected energy layers to get the treatment plan. For simplicity, treatment planning was with respect to PTV, which is sufficient for the purpose of this work. For fair comparison, both EM and ES were solved by FISTA and plans were normalized after optimization with  $D_{95} = 100\%$  at PTV. To simulate SPARC, we divided the full 360° arc into 72 equally segmented beam intervals of at 5°, and each interval was approximated by the beam angle at its center. Then the dose influence matrix  $A$  was generated via MatRad<sup>17</sup> using 5 mm lateral spacing, and 3 mm longitudinal spacing for energy discretization, on 3 mm-resolution dose grid.

In Table 1, the conformity index (CI) is defined as  $V_{100}^2 / (V \times V'_{100})$  ( $V_{100}$ : PTV volume receiving at least 100% of prescription dose;  $V$ : PTV volume;  $V'_{100}$ : total volume receiving at least 100% of prescription dose). The value of CI is between 0 and 1, with its optimal value being 1. The homogeneity index (HI)<sup>23</sup> is defined as  $(D_2 - D_{98}) / D_p \times 100\%$  ( $D_2$ : the min dose for 2% volume receiving the highest dose;  $D_{98}$ : the min dose for

98% volume receiving the highest dose;  $D_p$ : the prescription dose); smaller value of HI corresponds to a more homogeneous target dose.

The total plan delivery time  $T$  is estimated using a simplified beam delivery model that only accounts for energy switching time  $T_E$  and spot delivery time  $T_B$ . In Table 2,  $T_E$  is calculated assuming 5.5 s for each SU and 0.6 s for each SD, and  $T_B$  is estimated by  $T_B = \|x\|_1 / \gamma$ , with the dose rate  $\gamma = 2.6 \times 10^{10}$  protons/mins (this dose rate corresponds to the minimum MU threshold  $1.1 \times 10^6$  protons for the Varian ProBeam system).

## 3 | RESULTS

### 3.1 | EM had fewer SU than ES

The energy-layer delivery trajectories optimized with ES and EM are presented in Figure 4, which shows that EM had fewer SU than ES. Specifically, compared to ES, EM reduced SU from 36 to 13 for abdomen, from 31 to 26 for brain, from 35 to 24 for HN, from 32 to 24 for lung, with an average of 35% reduction of SU. Also, note that ES was strictly one energy layer per angle, while EM removed such striction and allowed more than one energy layers per angle. This flexibility in the number of energy layers per angle can allow for the improvement in plan quality, which will be presented in the next section.

### 3.2 | EM had better plan quality than ES

For plan quality comparison, dosimetric parameters are summarized in Table 1, dose volume histogram (DVH) plots and dose plots are presented in Figures 5 and 6, respectively. As shown in Table 1, EM had smaller optimization objective values than ES, which indicates that EM had better plan quality than ES. Moreover, EM provided better target dose conformality, indicated by larger CI values, for example, an increase from 0.53 to 0.84 for Brain in Table 1; EM provided better target dose homogeneity, indicated by smaller HI values, example, a decrease from 15.14 to 9.34 for lung in Table 1; EM had generally lower dose to OAR and lower integral dose to body. The improved plan quality via EM is also demonstrated by DVH plots in Figure 5 and dose plots in Figure 6: EM had steeper target DVH curve and lower OAR DVH curve in Figure 5, and tighter 80% isodose line in Figure 6.

### 3.3 | EM was more efficient than ES

As shown in Table 2, EM had shorter energy switching time  $T_E$  than ES, due to reduced number of SU, despite of increased number of SD. On the other hand, EM also had shorter spot delivery time  $T_B$  than ES. As a result,

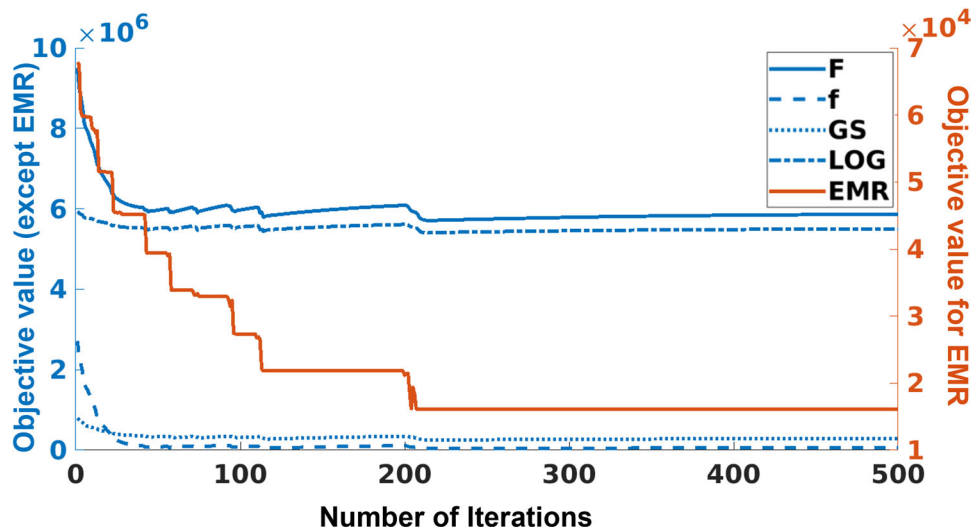


**FIGURE 7** Convergence plot of EM for the brain case.  $F$ : total objective;  $f$ : dose fidelity; GS: group sparsity term; LOG: log barrier term; EMR: energy matrix term. Note that the  $y$ -axis for EMR is different from the rest terms

EM had shorter total plan delivery time  $T$  and thus was more efficient than ES. Specifically, compared with ES, EM reduced total plan delivery time  $T$  from 307 to 140 s (54% reduction) for abdomen, from 252 to 217 s (14% reduction) for brain, from 460 to 359 s (22% reduction) for HN, from 415 to 339 s (18% reduction) for lung, with an average of 23% reduction of total delivery time.

### 3.4 | EM was more computationally efficient than ES

Regarding the number of iterations, ES converged in 1000–1500 iterations to meet the one-energy-layer-per-beam requirement, while EM converged in 500 iterations or fewer (e.g., Figure 7). Regarding computational cost per iteration, one EM iteration was one tenth of one ES iteration. The average run time of 500 ES iterations took about 6000 s, while that of 500 EM iterations took about 600 s, on a desktop computer with i5-11400 6-core 12-thread CPU. Therefore, EM was more computationally efficient than ES by at least 10-fold.

## 4 | DISCUSSION

It is an intrinsic tradeoff between plan quality and delivery efficiency, even for SPARC, regardless of ES or EM. However, as demonstrated in *Result* section, compared with ES, EM improved both delivery efficiency (with reduced number of SU) and plan quality. Therefore, EM has a better tradeoff than ES, that is, lower Pareto surface in terms of multicriteria optimization.

In term of algorithm difference for SU reduction, ES requires the calculation of several regularization

matrices each FISTA iteration, which substantially slows down the ES method; on the other hand, ES has to impose the condition “one energy layer per angle” in order to for ES to function. In contrast, the  $M$  matrix in EM is computed only once, and thus its computational cost is negligible overall; EM does not need to be constrained by the ES condition and can have more than one energy layer per angle, and the removal of the constraint allows EM to have more optimization degrees of freedom to improve plan quality. On the other hand, there is a flaw for EM that the  $M$  matrix can have unnecessary penalization to some energy layers. For example, considering the scenario that SU occurs at the current angle (i.e., the leading energy layer at this angle has larger energy than the smallest energy layer of the previous angle), although the selection of other energy layers at this angle does not further increase SU with respect to the previous angle, the  $M$  matrix still penalizes the selection of remaining energy layers, which is unnecessary. However, this flaw seems practically minor, as EM still outperformed ES in plan quality.

We have tried both ADMM and FISTA and found no major difference in results. However, since FISTA was used in the original ES paper,<sup>8</sup> we also adopt FISTA here. On the other hand, we found the difference between  $\frac{1}{2}$  norm and L1 norm for GS is negligible; given the L1 norm is more common for GS, we also use L1-norm based GS term in this work.

Without complicating the matter of this work on ELO, we have not considered the minimum monitor-unit (MMU) constraint, that is, MMU optimization problem, that may be needed for SPARC plans to be deliverable. It should be technically straightforward to add MMU to ELO for either ES and EM, for example, to incorporate our previous MMU methods.<sup>18–21</sup> However, MMU-based

SPArc treatment planning can be practically challenging, as the MMU constraint is nonconvex and more restrictive for SPArc than IMPT. That is, since SPArc has more optimization degrees of freedom and thus smaller monitor units per spot, the MMU constraint is harder to meet for SPArc, for which a recently developed MMU method<sup>22</sup> for relatively large MMU threshold may help.

## 5 | CONCLUSION

We have developed a new ELO method for SPArc using EMR and shown that this new method EM can improve both delivery efficiency and plan quality, with substantially enhanced computational efficiency, compared with a state-of-the-art method ES.

## ACKNOWLEDGMENTS

The authors are very thankful to the valuable comments from anonymous reviewers. This research is partially supported by NIH grants No. R37CA250921, R01CA261964, and a KUCC physicist-scientist recruiting grant.

## CONFLICT OF INTEREST

The authors have no conflicts to disclose.

## REFERENCES

- Deasy J, Mackie T, DeLuca P. Method and apparatus for proton therapy. 1997.
- Sandison GA, Papiez E, Block C, et al., Phantom assessment of lung dose from proton arc therapy. *Int J Radiat Oncol Biol Phys.* 1997;38:891–897.
- Ding X, Li X, Zhang JM, et al., Spot-scanning proton arc (SPArc) therapy: the first robust and delivery-efficient spot-scanning proton arc therapy. *Int J Radiat Oncol Biol Phys.* 2016;96:1107–1116.
- Li X, Kabolizadeh P, Yan D, et al., Improve dosimetric outcome in stage III non-small-cell lung cancer treatment using spot-scanning proton arc (SPArc) therapy. *Radiat Oncol.* 2018;13:35.
- Ding X, Li X, Qin A, et al., Have we reached proton beam therapy dosimetric limitations?—A novel robust, delivery-efficient and continuous spot-scanning proton arc (SPArc) therapy is to improve the dosimetric outcome in treating prostate cancer. *Acta Oncol (Madr).* 2018;57:435–437.
- Ding X, Zhou J, Li X, et al., Improving dosimetric outcome for hippocampus and cochlea sparing whole brain radiotherapy using spot-scanning proton arc therapy. *Acta Oncol (Madr).* 2019;58:483–490.
- Li X, Liu G, Janssens G, et al., The first prototype of spot-scanning proton arc treatment delivery. *Radiother Oncol.* 2019;137:130–136.
- Gu Wenbo, et al., A novel energy layer optimization framework for spot-scanning proton arc therapy. *Med Phys.* 2020;47.5, 2072–2084.
- Gao H, Hybrid proton-photon inverse optimization with uniformity-regularized proton and photon target dose. *Phys Med Biol.* 2019;64:105003.
- Gao H, Lin B, Lin Y, et al., Simultaneous dose and dose rate optimization (SDDRO) for FLASH proton therapy. *Med Phys.* 2020;47:6388–6395.
- Gao H, Liu J, Lin Y, et al., Simultaneous dose and dose rate optimization (SDDRO) of the FLASH effect for pencil-beam-scanning proton therapy. *Med Phys.* 2022;49:2014–2025.
- Gu W, O'Connor D, Nguyen D, et al., Integrated beam orientation and scanning-spot optimization in intensity-modulated proton therapy for brain and unilateral head and neck tumors. *Med Phys.* 2018;45:1338–1350.
- Beck A, Teboulle M, A Fast Iterative Shrinkage-Thresholding Algorithm for Linear Inverse Problems. *SIAM J Imaging Sci.* 2009;2:183–202.
- Boyd S, Parikh N, Chu E, et al., Distributed optimization and statistical learning via the alternating direction method of multipliers. *Found Trends® Mach Learn.* 2011;3:1–122.
- Goldstein T, and Osher S, The split Bregman algorithm for l1 regularized problems. *SIAM J Imaging Sci.* 2009;2:323–343.
- Parikh N, and Boyd S, “Proximal algorithms.” *Found Trends® Mach Learn.* 2014;1(3), 127–239.
- Wieser HP, Cisternas E, Wahl N, et al., Development of the open-source dose calculation and optimization toolkit matRad. *Med Phys.* 2017;44:2556–2568.
- Lin Y, Kooy H, Craft D et al., A Greedy reassignment algorithm for the PBS minimum monitor unit constraint. *Phys Med Biol.* 2016;61:4665–4678.
- Gao H, Clasié BM, Liu T et al., Minimum MU optimization (MMO): an inverse optimization approach for the PBS minimum MU constraint. *Phys Med Biol.* 2019;64:125022.
- Lin Y, Clasié BM, Liu T et al., Minimum-MU and sparse-energy-level (MMSEL) constrained inverse optimization method for efficiently deliverable PBS plans. *Phys Med Biol.* 2019;64:205001.
- Gao H, Clasié BM, McDonald M et al., Plan-delivery-time constrained inverse optimization method with minimum-MU-per-energy-layer (MMPEL) for efficient pencil beam scanning proton therapy. *Med Phys.* 2020;47:3892–3897.
- Cai JF, Chen RC, Fan J, and Gao H, Minimum-monitor-unit optimization via a stochastic coordinate descent method. *Phys Med Biol.* 2022;67:015009.
- Wu Q, Mohan R, Morris M, et al., Simultaneous integrated boost intensity-modulated radiotherapy for locally advanced head-and-neck squamous cell carcinomas. I: dosimetric results. *Int J Radiat Oncol Biol Phys.* 2003;56:573–585.

**How to cite this article:** Zhang G, Shen H, Lin Y, Chen RC, Long Y, Gao H. Energy layer optimization via energy matrix regularization for proton spot-scanning arc therapy. *Med Phys.* 2022;49:5752–5762.

<https://doi.org/10.1002/mp.15836>